Bioelectrochemistry 91 (2013) 1–7

Contents lists available at SciVerse ScienceDirect

Bioelectrochemistry

journal homepage: www.elsevier.com/locate/bioelechem

Nanomaterial-based electrochemical biosensors for cytochrome *c* using cytochrome *c* reductase

Manickam Pandiaraj [a], Thangamuthu Madasamy [a], Paradesi Naidu Gollavilli [b], Murugesan Balamurugan [a], Srigiridhar Kotamraju [b], Vepa Kameswara Rao [c], Kalpana Bhargava [d], Chandran Karunakaran [a,*]

[a] *Biomedical Research Laboratory, Department of Chemistry, VHNSN College, Virudhunagar-626001, Tamil Nadu, India*
[b] *Center for Chemical Biology, Indian Institute of Chemical Technology, Hyderabad-500607, India*
[c] *Defence Research & Development Establishment, Gwalior, Madhya Pradesh-474002, India*
[d] *Peptide and Proteomics Division, DIPAS-DRDO, Delhi-110054, India*

ARTICLE INFO

Article history:
Received 27 July 2012
Received in revised form 5 September 2012
Accepted 29 September 2012
Available online 7 November 2012

Keywords:
Cytochrome *c* reductase
Cytochrome *c* quantification
Apoptosis
Gold nanoparticles
Carbon nanotubes

ABSTRACT

Emerging evidences have pointed out that the release of cytochrome *c* (cyt *c*) from mitochondria into cytosol is a critical step in the activation of apoptosis. This article presents a novel approach for the detection of mitochondrial cyt *c* release for the first time using cytochrome *c* reductase (CcR) immobilized on nanoparticles decorated electrodes. Two kinds of nanomaterial-based biosensor platforms were used: (a) carbon nanotubes (CNT) incorporated polypyrrole (PPy) matrix on Pt electrode and (b) self-assembled monolayer (SAM) functionalized gold nanoparticles (GNP) in PPy-Pt. Scanning electron microscope was used to characterize the surface morphologies of the nanomaterial modified electrodes. Cyclic voltammograms of both the biosensors showed reversible redox peaks at −0.45 and −0.34 V *vs* Ag/AgCl, characteristic of CcR. In comparison, the CcR-CNT biosensor gave a detection limit of 0.5 ± 0.03 μM cyt *c*, which was 4-fold better than the CcR-GNP biosensor (2 ± 0.03 μM). Moreover, the CcR-CNT biosensor achieved a much larger linear range (1–1000 μM) over the CcR-GNP biosensor (5–600 μM) with 2-fold better sensitivity. The CcR-CNT-PPy-Pt biosensor was further applied to quantify the mitochondrial cyt *c* released in cytosol of A549 cells upon induction of apoptosis with doxorubicin, the results agreed well with standard western blot analysis.

1. Introduction

Cytochrome *c* (cyt *c*) is a heme containing metalloprotein located in the intermembrane space of mitochondria. It plays key physiological role in biological respiratory chain, whose function is to transfer electrons between cytochrome *c* reductase (complex III) and cytochrome *c* oxidase (complex IV) [1,2]. Mitochondria are the powerhouse of cells, known to play a central role in cell homeostasis. When mitochondria are damaged under pathological conditions, cyt *c* is released into the cytosol of the cells [3]. This translocation of cyt *c* from mitochondria to cytosol is a critical event in the activation of intracellular signaling; it results in a cascade of caspase activation and leads to programmed cell death-apoptosis [3,4]. Thus, the quantification of cyt *c* release as a biomarker of apoptosis could be of great important in clinical diagnosis and therapeutic research.

Currently, conventional methods such as spectrofluorimetry [5], spectroscopy [6], HPLC [7,3], flow cytometry [8], western blot, and enzyme linked immunosorbent assay (ELISA) [9–11] are widely used to detect the cyt *c* release. Although these methods have high sensitivity, unfortunately, they are multi-step and time consuming processes, require large, expensive instrument, extensive pre-treatment of the sample and also not suitable for rapid routine use. Electrochemical biosensors have emerged recently as an alternative tool for rapid and real-time analysis of clinically relevant analytes. Recently, Zhao et al. [12] and Liu et al. [13] have reported the amperometric sensors for the determination of cyt *c* with good detection limits. These methods, however, suffer from lack of selectivity for the quantification of cyt *c*, especially in cells or biological samples, due to the fact that the interaction of the recognition elements *viz.* single-strand DNA functionalized gold nanoparticles [12] and lauric acid modified lipid bilayer (negative charge) [13] with the cyt *c* (positive charge) is purely based on electrostatic interaction. These methods are prone to interferences by other positively charged species present in the samples and hence are not applicable for the measurement of cyt *c* release in biological systems. Enzymatic biosensors for the determination of cyt *c* have also been investigated by incorporating cytochrome *c* oxidase (CcO) [14,15]. However, the CcO based biosensors are capable of measuring only the reduced form of cyt *c* (Fe^{2+}) by mediating electron transfer between the cyt *c* (Fe^{2+}) and the electrode. But in apoptotic cells, only the oxidized form of cyt *c* (Fe^{3+}) triggers the time dependent caspase activation and serves as a proapoptotic molecule [16]. Moreover, in

* Corresponding author at: Biomedical Research Laboratory, VHNSN College, Virudhunagar—626001, Tamil Nadu, India. Tel.: +91 4562 280154; fax: +91 4562 281338.
E-mail address: ckaru2000@gmail.com (C. Karunakaran).

1567-5394/$ – see front matter © 2012 Elsevier B.V. All rights reserved.
http://dx.doi.org/10.1016/j.bioelechem.2012.09.004

permeablized cell models, the cytosolic cyt *c* (Fe^{2+}) is rapidly oxidized (Fe^{3+}) by the mitochondrial CcO [17], thus making the CcO based biosensors difficult to quantify the apoptotic form of cyt *c* (Fe^{3+}). In addition, upon immobilization, it is reported that the electron transfer is blocked in active centers of the CcO [18]. Consequently, the analytical applications of CcO based biosensors are limited. Thus, there is a real need for simple, rapid, selective and inexpensive methods for cyt *c* (Fe^{3+}) measurement for point-of-care and research applications.

So, in the present study, an alternate biosensor for the quantification of cyt *c* release in apoptotic cells has been developed by immobilizing cytochrome *c* reductase (CcR). CcR is a specific and complex redox enzyme with 3 subunits, catalyzing one electron reduction of oxidized cyt *c* (Fe^{3+}) [19]. The most crucial step in the development of biosensor is the immobilization of such biomolecules without affecting their native structures and bioactivities at the electrode surface. Indeed, the direct electron transfer of redox proteins is very difficult at conventional electrodes, since the active sites are deeply embedded in protein structure. Recently, conducting polymer, polypyrrole (PPy) has been used as a suitable host matrix for the immobilization of enzymes owing to its unique combinations of well-ordered conductive polymer chain and good environmental stability [20–22]. Further, the research has extended to modify PPy with other nanomaterials *viz*. carbon nanotubes (CNT) and gold nanoparticles (GNP) so as to obtain enhanced electron transfer of bioactive molecules in various biosensors [23–26]. CNT are novel molecular nanowires with high mechanical, chemical and electrical properties [27,28]. The morphology of CNT is extremely important in establishing the direct electrical contact between the redox protein and the electrode. Moreover, the modification of GNP surface with thiols provides a well ordered, compact and stable self-assembled monolayer (SAM) used to conjugate enzymes close to the electrode surface.

In this article, for the first time, we report cyt *c* biosensors based on immobilization of CcR on two kinds of nanomaterial decorated electrodes *viz*. CNT incorporated PPy modified Pt electrode and SAM of cysteine functionalized GNP on PPy modified Pt. The incorporation of CNT/GNP into the PPy matrix exhibited nanoporous structures with large effective surface area for the immobilization of CcR thereby enhanced the enzyme biocatalytic activity for the sensitive determination of cyt *c*. Further, the levels of mitochondrial cyt *c* released in cytosolic fractions of doxorubicin (DOX) treated human lung carcinoma A549 cells determined using the CcR-CNT-PPy-Pt biosensor were found to be in good agreement with the standard western blot analysis.

2. Material and methods

2.1. Reagents

Cyt *c* from bovine heart, CcR from porcine heart, cyt *c* monoclonal antibody, bovine serum albumin (BSA), DOX, chloroauric acid trihydrate ($HAuCl_4.3H_2O$), cysteine, glutaraldehyde, pyrrole, sodium hydrogen phosphate, disodium hydrogen phosphate and hydroquinone were purchased from Sigma (St. Louis, MO, USA). Single walled CNT were purchased from Carbon solutions Inc., CA, USA. Human lung carcinoma A549 cells were obtained from ATCC. All the solutions were prepared with doubly distilled water.

2.2. Instrumentations

All electrochemical experiments were carried out using CHI 1200B electrochemical workstation (CHI, USA) with a conventional three electrode system which consisted of an Ag/AgCl wire as reference electrode, a Pt wire as auxiliary or counter electrode and CcR immobilized/conjugated CNT-PPy-Pt and SAM-GNP-PPy-Pt electrode as working electrodes. The size of Pt working electrode used was 0.5 mm in diameter. The morphological scanning electron microscopic (SEM) images and energy dispersive X-ray analysis (EDX) spectra were obtained using a FEI Quanta FEG 200-High Resolution Scanning Electron Microscope (FEI Co., Netherlands). The phase contrast images were acquired by using an Olympus-1X71 inverted microscope (Olympus Co., USA).

2.3. Construction of CcR-SAM-GNP-PPy-Pt biosensor

Pyrrole was first electropolymerized onto the bare Pt electrode to form PPy matrix by following the reported procedure [24]. The optimum of 10 cycles for pyrrole electropolymerization was used because of its increased conductivity and large surface area as reported earlier [20] for the effective incorporation of CNT, GNP and enzyme.

GNP of diameter around 6–10 nm was prepared according to a previously published route [29]. The prepared GNP was characterized by UV–vis spectroscopy (data not shown). The obtained PPy-Pt electrode was immersed in GNP solution for 12 h and carefully rinsed with double distilled water. The GNP-PPy-Pt electrode modified with the SAM of cysteine was prepared by dipping the GNP incorporated PPy-Pt electrode into a 1 mM cysteine solution for 10 min and rinsed with double distilled water to remove the non-chemisorbed cysteine. Then 5 μL of CcR (0.2 g/mL) solution was dropped onto the SAM-GNP-PPy-Pt electrode by employing 5 μL of glutaraldehyde (GA) (2.5%) solution as cross-linking agent. After that, the electrode was left for at least 24 h at room temperature for efficient cross-linking. During this process, CcR was conjugated to the SAM-GNP-PPy-Pt electrode.

2.4. Construction of CcR-CNT-PPy-Pt biosensor

The CNT modified PPy-Pt electrode was prepared by the reported procedure [24]. In brief, 25 μL of CNT solution (2 ml of 1.5 wt% nafion–ethanol solution containing 2 mg of CNT) was dropped on PPy-Pt electrode surface, and then the solvent ethanol was evaporated in air to form a CNT incorporated PPy-Pt electrode. The immobilization of CcR on CNT-PPy-Pt electrode was carried out as described before similar to SAM-GNP-PPy-Pt. Later, the CcR immobilized electrode was kept for at least 24 h at room temperature for efficient cross-linking and entrapment of the CcR on the CNT-PPy-Pt electrode. The above constructed cyt *c* biosensors were illustrated in Scheme 1A.

2.5. Culture of human lung carcinoma A549 cells and doxorubicin treatment

Human lung carcinoma A549 cells were grown in 10% Dulbeccos modified Eagle's medium containing 10% fetal bovine serum, l-glutamine (4 mM/L), penicillin (100 units/mL), and streptomycin (100 μg/mL), and incubated at 37 °C in a humidified atmosphere of 5% CO_2. In order to induce apoptosis, cells were treated with 1 μM DOX for a period of 0–48 h. Cytosolic fractions of the cells were prepared according to the manufacturer's instructions using QIA88 Proteoextract cytosol/mitochondria fractionation kit from Calbiochem.

2.6. SDS-PAGE and western blot analysis of cyt c

The DOX-treated and untreated cells were harvested and washed twice with PBS and lysed in a lysis buffer for 10 min and centrifuged at 12,000 g for 10 min at 4 °C. The total protein was determined by Bradford protein assay. For western blotting, the proteins were separated by 12% SDS-PAGE and transferred onto nitrocellulose membrane. The membrane was then blocked with 2% BSA in tris-buffered saline for inhibition of non-specific binding and then incubated with anti-cyt *c* antibody (1:500) overnight at 4 °C. Alkaline phosphatase-conjugated anti-chicken IgG antibody was used to detect the signal by BCIP/NBT method.

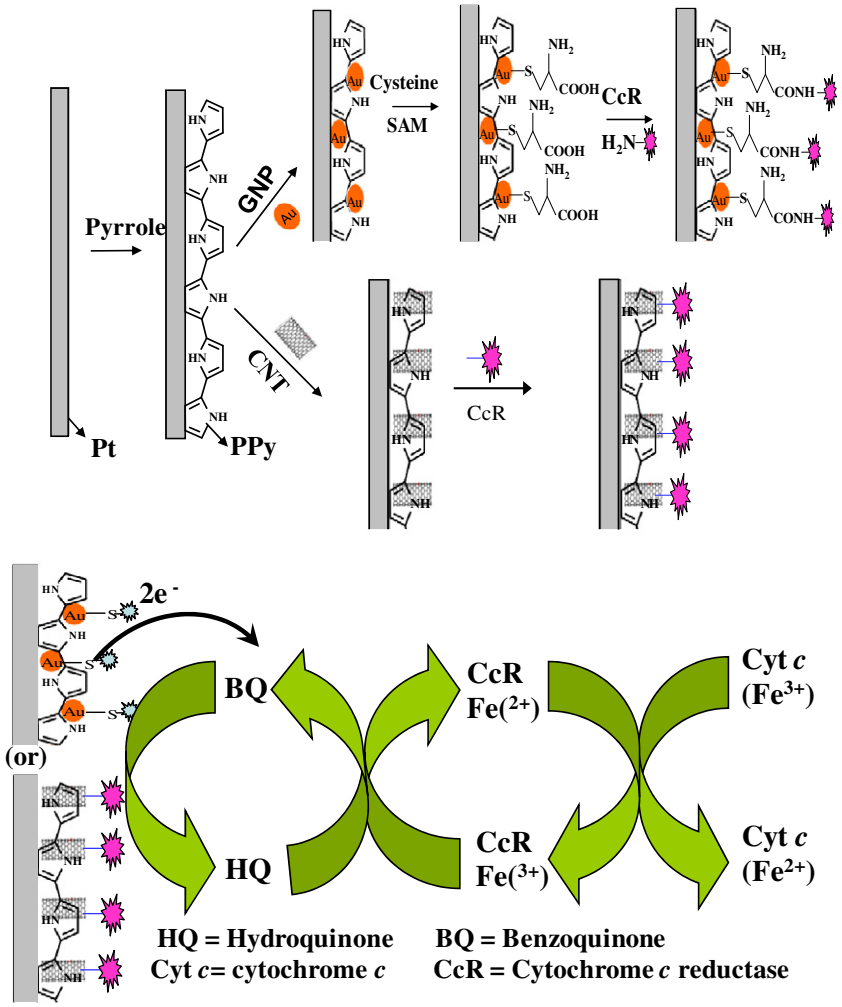

Scheme 1. A: Schematic representation of the CcR based cyt *c* biosensors. B: Schematic illustration of the biochemical reaction occurring at the biosensors surface.

3. Results and discussion

CcR is an essential segment in the electron transport chain of mitochondria, playing a critical role in the biochemical generation of ATP [30]. It specifically reduces the cyt *c* (Fe^{3+}) by the oxidation of ubiquinol (QH_2) into ubiquinone (Q). CcR is a complex enzyme composed of three major subunits with redox prosthetic groups: a di-heme cyt *b* containing a relatively high-potential b_H heme and a lower potential b_L heme, cyt c_1 and a Rieske iron–sulphur protein with a 2Fe–2S cluster [19]. To enhance the fast electron transfer between the deeply embedded multi-redox centers of CcR and the electrode, we have used here the synergistic effects of GNP and CNT incorporated PPy nanocomposite matrix. These two kinds of nanomaterial tailored PPy platforms anchored the CcR well and facilitated the direct electron transfer to achieve high sensitivity for the specific quantification of cyt *c* release in cancer cells.

3.1. SEM characterization of the modified electrodes

The morphological images of the GNP-PPy-Pt and CNT-PPy-Pt electrodes investigated by SEM are shown in Fig. 1. The SEM image of GNP-PPy-Pt electrode (Fig. 1a) reveals the incorporated GNP onto the microporous matrix of PPy-Pt. This perhaps increases the specific surface area available on the PPy-Pt electrode for the efficient conjugation of CcR. Further, Fig. 1c revealed the existence of well dispersed CNT in the PPy film. These conductive and porous CNT further provided a biocompatible and advantageous platform for the immobilization of more number of CcR to achieve increased sensitivity.

3.2. Electrochemical characterization of the biosensors

Fig. 2 exhibits the typical cyclic voltammograms (CVs) of the modified electrodes in 0.1 M PBS (pH 7.0) at a scan rate of 50 mVs^{-1}. There were no significant redox peaks obtained for bare Pt (Fig. 2a), PPy-Pt (Fig. 2b) and CNT-PPy-Pt (Fig. 2c) electrodes. On the other hand, CcR immobilized on PPy-Pt (Fig. 2d) and CNT-PPy-Pt (Fig. 2e) electrodes showed well defined reversible redox peaks at −0.45 and −0.34 V *vs* Ag/AgCl. As with the CNT platform, the CcR conjugated to SAM on GNP-PPy-Pt electrode also exhibited the similar redox peaks at −0.45 and −0.34 V *vs* Ag/AgCl (Fig. S1, Supplementary material). These redox peaks obtained here for the immobilized CcR are akin to CcR observed in solution (data not shown). Further, experimental evidences indicate that the domain [2Fe–2S], the primary electron acceptor present in the active site, moves between cyt *b* and cyt c_1 resulting in fast electron transfer within the CcR [31–33]. So, the observed reversible redox peaks at −0.45 and −0.34 V here presumably ascribed to the redox reactions of [2Fe–2S] iron–sulphur cluster present in the active site of the CcR. The characteristic peaks obtained here for CcR were quite similar to [2Fe–2S] proteins reported in earlier studies [34,35]. These investigations clearly suggested that the redox peaks observed here at −0.45 and −0.34 V were attributed to the electron transfer reaction of the immobilized CcR with the modified electrodes.

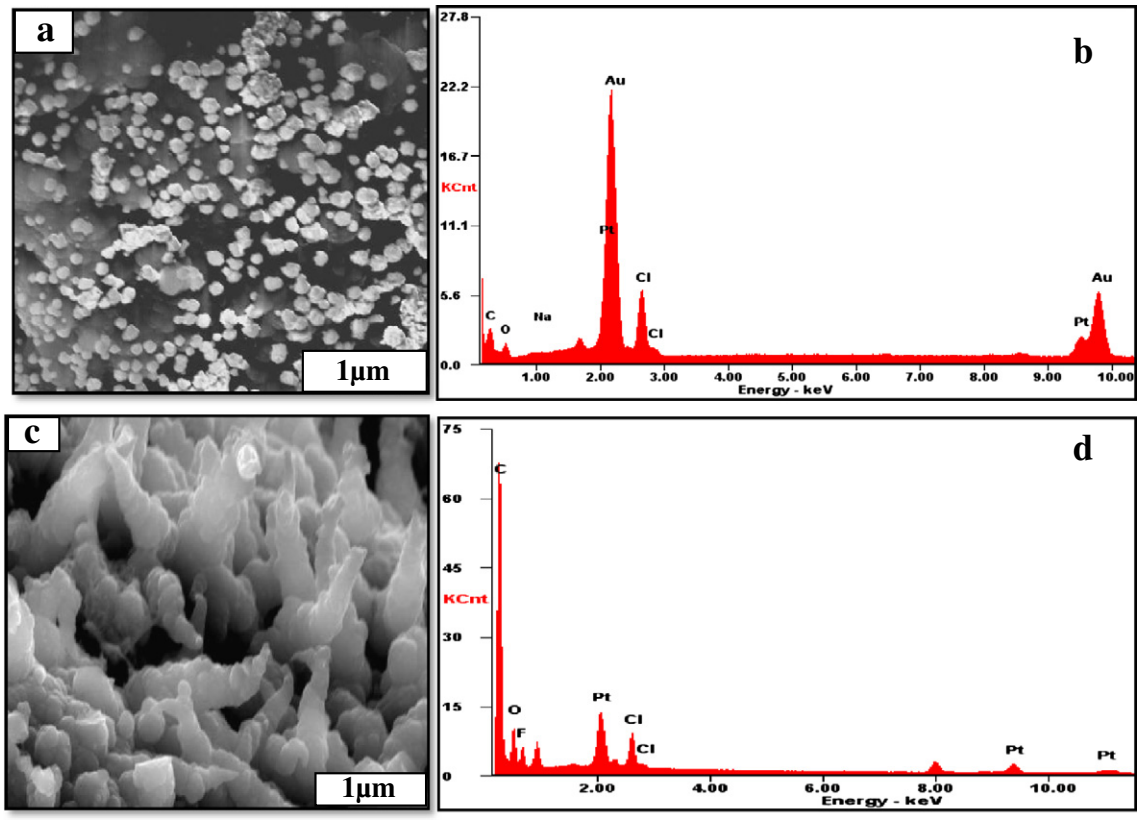

Fig. 1. SEM images of (a) GNP-PPy-Pt and (c) CNT-PPy-Pt and EDX spectrum of (b) GNP-PPy-Pt and (d) CNT-PPy-Pt electrodes.

3.3. Electrochemical response to cyt c

The coupling of oxidation–reduction and deprotonation–protonation of QH_2 with the CcR is the central mechanism in cyt *c* reduction [36]. So, we used here hydroquinone (HQ) as a mediator for the reduction of cyt *c* by CcR. The current responses for the CcR-CNT-PPy-Pt biosensor were studied in 0.1 M PBS (pH 7.0) containing 100 µM cyt *c* in different concentrations of HQ. The current increased sharply with increasing HQ concentrations to a maximal response at 0.5 mM, and then became steady with the further increase in HQ concentrations (Fig. S2, Supplementary material). Thus, the optimized 0.5 mM HQ was used for our experiments.

Fig. 3 displays the CVs obtained for CcR-SAM-GNP-PPy-Pt (dotted lines) and CcR-CNT-PPy-Pt electrodes (solid lines) in 0.1 M PBS containing 0.5 mM HQ in the absence and presence of 500 µM cyt *c*. In both the cases, before the addition of cyt *c*, characteristic redox peaks (−0.45 and −0.34 V *vs* Ag/AgCl) due to the immobilized CcR were observed (*vide supra*). Upon addition of cyt *c*, the current increased cathodically at −0.45 V and also anodically at −0.34 V, which was attributed to the redox reaction of cyt *c* by the CcR. Under similar conditions, there were no changes in CV responses observed for the PPy-Pt, GNP-PPy-Pt and CNT-PPy-Pt electrodes. However, for these electrodes (without CcR) in the presence of cyt *c*, new reversible redox peaks appeared at 0.05 and 0.07 V *vs* Ag/AgCl, characteristics of cyt *c* [37]

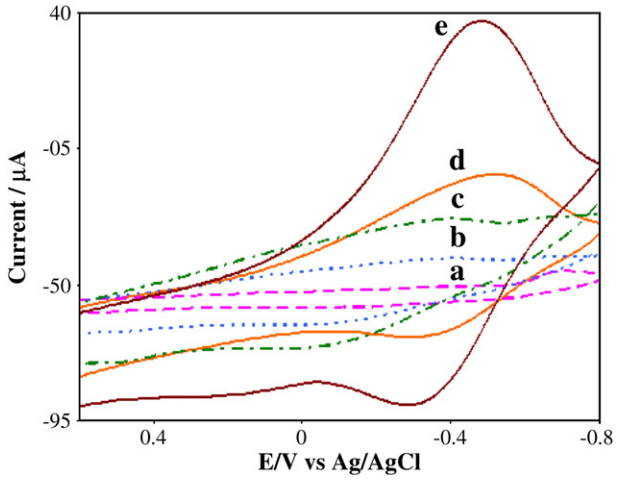

Fig. 2. Typical CV responses of (a) bare Pt, (b) PPy-Pt, (c) CNT-PPy-Pt, (d) CcR-PPy-Pt and (e) CcR-CNT-PPy-Pt electrodes in 0.1 M PBS at pH 7.0 containing 100 µM DTPA; scan rate: 50 mVs^{-1} *vs* Ag/AgCl.

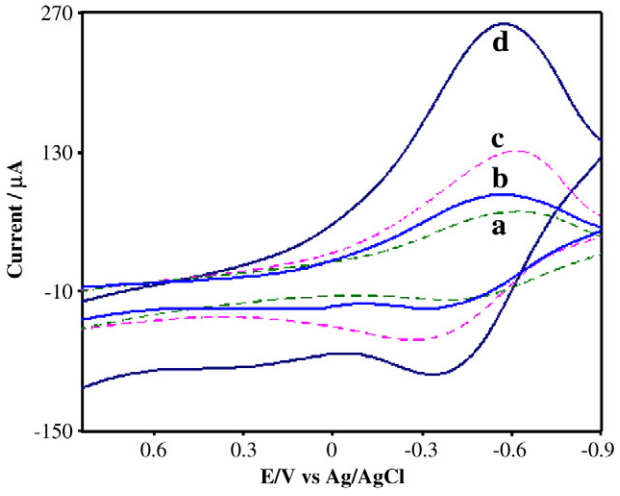

Fig. 3. CVs obtained for CcR-SAM-GNP-PPy-Pt (dotted lines) and CcR-CNT-PPy-Pt (solid lines) electrodes in the absence (a and b) and in the presence (c and d) of 500 µM of cyt *c* respectively in 0.1 M PBS containing 0.5 mM HQ; scan rate: 50 mVs^{-1} *vs* Ag/AgCl.

(data not shown), whereas, the peaks due to cyt *c* were not exhibited by the CcR immobilized electrodes. Therefore, the increases in current responses at −0.45 and −0.34 V are mainly due to the redox reaction of cyt *c* by the CcR but not due to the cyt *c* in solution. The present data thus confirms the immobilized CcR showing an enhanced biocatalytic activity towards the reduction of cyt *c* (Fe^{3+}). The schematic representation of the biochemical reaction of the CcR with cyt *c* occurring at the electrodes surface is shown in Scheme 1B.

3.4. Comparison of effect of CNT/GNP on the performance of the biosensor

Typical CVs obtained for CcR-PPy-Pt (a), CcR-SAM-GNP-PPy-Pt (b) CcR-CNT-PPy-Pt (c) electrodes in 0.1 M PBS in the presence of 500 μM of cyt *c* containing 0.5 mM HQ were compared in Fig. 4. It is clearly seen that the CVs of the CcR-SAM-GNP-PPy-Pt and CcR-CNT-PPy-Pt electrodes showed huge increase in currents at −0.45 and −0.34 V *vs* Ag/AgCl than that of the CcR-PPy-Pt. The remarkable increase in currents can be attributed to the large number of CcR firmly immobilized on the electroactive nanoporous surfaces provided by the GNP/CNT in PPy than in the microporous PPy matrix. Further, the CcR-CNT biosensor exhibited nearly 2-fold increase in current than the CcR-GNP biosensor. This higher increase in the current for CNT platform maybe explained due to its high electrical conductivity and fast electron transfer. Also, the nanoscale contours of these nanotubes perhaps penetrated slightly into the CcR thereby lowering the electron transfer distance between the electrode and the various active sites of the CcR.

3.5. Selectivity of the cyt c biosensor

Ascorbic acid (AA) and uric acid (UA) are considered to be the major interferants to most biosensors because of their relatively high concentrations in biological samples and low oxidation potentials [25]. The interferences were investigated by comparing the current responses before and after the additions of 500 μM each of AA and UA in the presence of 250 μM cyt *c* containing 0.1 M PBS. It was observed that only AA caused observable interference in the determination of cyt *c* (data not shown). In order to remove the interference due to AA, the mixture of cyt *c* and AA was dialyzed by immersing it in 0.1 M PBS. Since, cyt *c* was too large (12.3 kDa) to pass through the membrane, only AA moves across the membrane. Then, the retentate of the dialysis was analyzed. The CVs thus obtained for the retentate using the cyt *c* biosensors did not show any observable interference due to AA. The effects of scan rate and pH on the performance of the CcR-CNT-PPy-Pt biosensor investigated are shown in Fig. S3A and B respectively (Supplementary material).

3.6. Linear range, minimum detectable concentration and stability

The typical CVs obtained for several concentrations of cyt *c* in 0.1 M PBS containing 0.5 mM HQ using these two cyt *c* biosensors at 50 mVs^{-1} are shown in Figs. 5 and S4. The current responses to cyt *c* obtained with the CcR-CNT-PPy-Pt biosensor (Fig. 5) was linear from 1–1000 μM ($r^2 = 0.997$), with a detection limit of 0.5 ± 0.03 μM and sensitivity of 0.46 ± 0.003 μA μM^{-1} cm^{-2}. On the other hand, the current responses obtained with the CcR-SAM-GNP-PPy-Pt biosensor (Fig. S4, Supplementary material) was only linear from 5 to 600 μM ($r^2 = 0.995$) with a detection limit of 2 ± 0.03 μM and showed a sensitivity of 0.24 ± 0.004 μA μM^{-1} cm^{-2}. The detection limits of these biosensors are well below the lowest physiological concentration of cyt *c* previously reported [38,39]. On comparing the results obtained for CcR-SAM-GNP-PPy-Pt biosensor with CcR-CNT-PPy-Pt, the latter exhibited a wide linear range, lower detection limit and nearly 2-fold higher sensitivity for the cyt *c* determination.

The reproducibility of these cyt *c* biosensors was investigated in 0.1 M PBS containing 100 μM cyt *c* by repetitive determination of cyt *c* in triplicate. The results showed good reproducibility at the modified electrodes, with a relative standard deviation of 2.8%. For evaluating the stability of the biosensors, the cathodic current responses to cyt *c* were recorded three times daily and the responses were found to be constant for at least 4 weeks. Thus, the CNT as well as SAM on GNP in PPy matrix perhaps maintained the CcR activity well by providing an environment similar to that of the redox protein in a native system.

3.7. Measurement of cyt c release from mitochondria

An important step in the mitochondrial pathway is the release of cyt *c* from mitochondria into cytosol. It has been earlier demonstrated that the cyt *c* translocates from the mitochondria into cytosol preceded DOX-induced apoptosis in various cell and animal models [40,41]. So, we have chosen DOX for the induction of apoptosis in human lung carcinoma A549 cells. Recent findings revealed that the oxidized form of cyt *c* (Fe^{3+}) mainly induced the caspase activation thereby causing apoptosis over the reduced form of cyt *c* (Fe^{2+}) [17]. It clearly indicates that the measurement of only the oxidized form of cyt *c* (Fe^{3+}) in cytosol presumably serves as a marker for apoptotic process in cells. In this

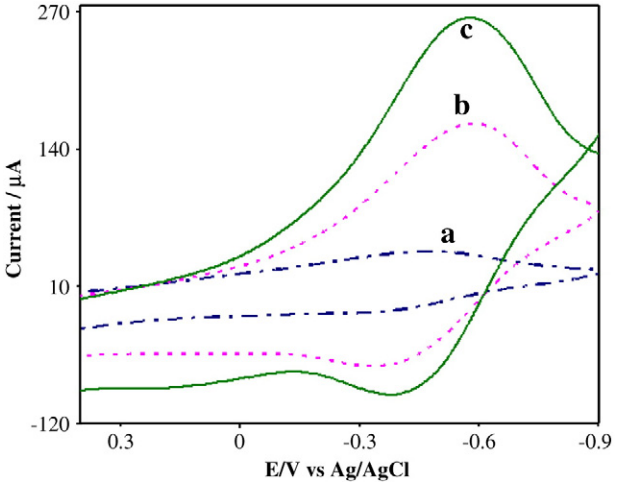

Fig. 4. CV responses of (a) CcR-PPy-Pt, (b) CcR-SAM-GNP-PPy-Pt and (c) CcR-CNT-PPy-Pt electrodes in the presence of 500 μM cyt *c* solution in 0.1 M PBS containing 0.5 mM HQ; scan rate: 50 mVs^{-1}.

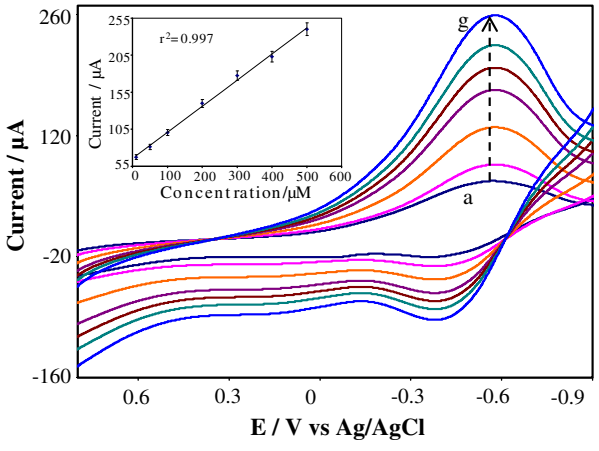

Fig. 5. Typical CV responses of the CcR-CNT-PPy-Pt electrode in 0.1 M PBS containing 0.5 mM HQ, without (a) and with 50, 100, 200, 300, 400, 500 μM of cyt *c* (b–g) measured at scan rate of 50 mVs^{-1}. A linear calibration plot of cathodic peak currents against cyt *c* concentrations (Inset of Fig. 5). Each point represents the mean (±0.03 SD) of three measurements.

report, cyt *c* (Fe^{3+}) measurements were performed on the cytosolic fractions of DOX treated and untreated human lung carcinoma apoptotic A549 cells using the CcR-CNT-PPy-Pt biosensor and western blot. After 24 h exposure of cells with 1 μM DOX, the cyt *c* concentration in cytosolic fractions of the cells (3.63 ± 0.02 μM) were increased when compared to those in untreated cells (2.4 ± 0.02 μM). Treatment for 48 h resulted in further increase in cytosolic cyt *c* (5.3 ± 0.018 μM) levels (Fig. S5A, Supplementary material). These results are quite comparable with the cell viability studies (Fig. S6, Supplementary material) and western blot analysis (Fig. S5B, Supplementary material).

4. Conclusion

Novel cyt *c* biosensors for the specific and sensitive determination of cyt *c* (Fe^{3+}), biomarker of apoptosis, were developed here by immobilizing for the first time CcR on CNT incorporated PPy-Pt and SAM of cysteine on GNP in the PPy-Pt matrix. The synergistic effect of CNT/GNP in conducting PPy matrix enhanced the direct electron transfer and catalytic activity of CcR by providing a well ordered, stable and large surface for the immobilization without affecting its biological activity. The CcR-CNT based biosensor achieved a very low detection limit, wide linear range and high sensitivity over the CcR-GNP based biosensor perhaps due to penetrating power of CNT thereby decreasing the electron-transfer distance between the various Fe (II/III) redox active sites of CcR and the base electrode. Furthermore, the CcR-CNT based cyt *c* biosensor was applied to quantify the cytosolic cyt *c* released from the mitochondria of apoptotic human lung carcinoma A549 cells and the results are in good agreement with the standard western blot analysis.

Abbreviations

AA	Ascorbic acid
CNT	Carbon nanotubes
Cyt *c*	Cytochrome *c*
CcO	Cytochrome *c* oxidase
CcR	Cytochrome *c* reductase
CV	Cyclic voltammetry
DOX	Doxorubicin
DTPA	diethylenetriaminepentaacetic acid
EDX	Energy dispersive X-ray spectroscopy
GA	Glutaraldehyde
GAPDH	Glyceraldehyde 3-phosphate dehydrogenase
GNP	Gold nanoparticles
HQ	Hydroquinone
kDA	Kilo Dalton
PBS	Phosphate buffer solution
PPy	Polypyrrole
PAGE	Polyacrylamide Gel electrophoresis
Q	Ubiquinone
QH_2	Ubiquinol
SAM	Self-assembled monolayer
SDS	Sodium dodecyl sulfate
SEM	Scanning electron microscopy
UA	Uric acid

Acknowledgments

This work was supported by the Department of Biotechnology, New Delhi, India (Grant No's. BT/PR13579/NNT/28/473/2010, BT/PR9637/BRB/10/582/2007) and the Managing Board of Virudhunagar Hindu Nadars' Senthikumara Nadar College, Virudhunagar, Tamil Nadu, India. Also, Ramanujan Fellowship to KS from DST, India is greatly acknowledged.

Appendix A. Supplementary data

Supplementary data to this article can be found online at http://dx.doi.org/10.1016/j.bioelechem.2012.09.004.

References

[1] Y.P. Ow, D.R. Green, Z. Hao, T.W. Mak, Cytochrome c: Functions beyond respiration, Nat. Rev. Mol. Cell Biol. 9 (2008) 532–542.
[2] M. Huttemann, P. Pecina, M. Rainbolt, T.H. Sanderson, V.E. Kagan, L. Samavati, J.W. Doan, I. Lee, The multiple functions of cytochrome *c* and their regulation in life and death decisions of the mammalian cell: From respiration to apoptosis, Mitochondrion 11 (2011) 369–381.
[3] J. Radhakrishnan, S. Wang, I.M. Ayoub, J.D. Kolarova, R.F. Levine, R.J. Gazmuri, Circulating levels of cytochrome *c* after resuscitation from cardiac arrest: A marker of mitochondrial injury and predictor of survival, Am. J. Physiol. Heart Circ. Physiol. 292 (2007) H767–H775.
[4] F. Zhou, S. Wu, B. Wu, W.R. Chen, D. Xing, Mitochondria-targeting single-walled carbon nanotubes for cancer photothermal therapy, Small 7 (2011) 2727–2735.
[5] Y. Shen, X.F. Yang, Y. Wu, C. Li, Sensitive spectrofluorimetric determination of cytochrome *c* with spirocyclic rhodamine B hydrazide in micellar medium, J. Flouresc. 18 (2008) 163–168.
[6] T. Nakashima, M. Sano, Single-walled carbon nanotube as 1D array of reacting sites: Reaction kinetics of reduction of cytochrome *c* in tris buffer, J. Phys. Chem. C 115 (2011) 20931–20936.
[7] E.D. Crouser, M.E. Gadd, M.W. Julian, J.E. Huff, K.M. Broekemeier, K.A. Robbins, D.R. Pfeiffer, Quantification of cytochrome *c* release from rat liver mitochondria, Anal. Biochem. 317 (2003) 67–75.
[8] B.L. Campos, B.A. Paim, R.G. Cosso, R.F. Castilho, H. Rottenberg, A.E. Vercesi, Method for monitoring of mitochondrial cytochrome *c* release during cell death: Immunodetection of cytochrome *c* by flow cytometry after selective permeabilization of the plasma membrane, Cytometry A 69 (A) (2006) 515–523.
[9] S. Kotamraju, E.A. Konorev, J. Joseph, B. Kalyanaraman, Doxorubicin-induced apoptosis in endothelial cells and cardiomyocytes is ameliorated by nitrone spin traps and ebselen, J. Biol. Chem. 275 (2000) 33585–33592.
[10] N.J. Waterhouse, J.A. Trapani, A new quantitative assay for cytochrome *c* release in apoptotic cells, Cell Death Differ. 10 (2003) 853–855.
[11] S. Kumar, S. Kasseckert, S. Kostin, Y. Abdallah, C. Schafer, A. Kaminski, H.P. Peter Reusch, H.M. Piper, G. Steinhoff, Y. Ladilov, Ischemic acidosis causes apoptosis in coronary endothelial cells through activation of caspase-12, Cardiovasc. Res. 73 (2006) 172–180.
[12] J. Zhao, X. Zhu, T. Li, G. Li, Self-assembled multilayer of gold nanoparticles for amplified electrochemical detection of cytochrome *c*, Analyst 133 (2008) 1242–1245.
[13] Y. Liu, W. Wei, Detection of cytochrome *c* at biocompatible nanostructured Au-lipid bilayer-modified electrode, Anal. Sci. 24 (2008) 1431–1436.
[14] J. Li, G. Cheng, S. Dong, Direct electron transfer to cytochrome c oxidase in self-assembled monolayers on gold electrodes, J. Electroanal. Chem. 416 (1996) 97–104.
[15] D. Ashe, T. Alleyne, E. Iwuoha, Serum cytochrome *c* detection using a cytochrome *c* oxidase biosensor, Biotechnol. Appl. Biochem. 46 (2007) 185–189.
[16] P. Pasdois, J.E. Parker, E.J. Griffiths, A.P. Halestrap, The role of oxidized cytochrome *c* in regulating mitochondrial reactive oxygen species production and its perturbation in ischaemia, Biochem. J. 436 (2011) 493–505.
[17] G.C. Brown, V. Borutaite, Regulation of apoptosis by the redox state of cytochrome *c*, Biochem. Biophys. Acta 1777 (2008) 877–881.
[18] J. Hrabakova, K. Ataka, J. Heberle, P. Hildebrandt, D.H. Murgida, Long distance electron transfer in cytochrome *c* oxidase immobilized on electrodes. A surface enhanced resonance Raman spectroscopic study, Phys. Chem. Chem. Phys. 8 (2006) 759–766.
[19] A.R. Crofts, J.T. Holland, D. Victoria, R.J. Kolling, S.A. Dikanov, R. Gilbreth, S. Lhee, R. Kuras, M.G. Kuras, The Q-cycle reviewed: How well does a monomeric mechanism of the bc_1 complex account for the function of a dimeric complex, Biochem. Biophys. Acta 1777 (2008) 1001–1019.
[20] S.S. Razola, B.L. Ruiz, N.M. Diez, H.B. Mark Jr., J.M. Kauffmann, Hydrogen peroxide sensitive amperometric biosensor based on horseradish peroxidase entrapped in a polypyrrole electrode, Biosens. Bioelectron. 17 (2002) 921–928.
[21] E.M.I. Ekanayake, D.M.G. Preethichandra, K. Kaneto, Bi-functional amperometric biosensor for low concentration hydrogen peroxide measurements using polypyrrole immobilizing matrix, Sens. Actuators B 132 (2008) 166–171.
[22] C.G. Aljaro, M.A. Bangar, E. Baldrich, F.J. Munoz, A. Mulchandani, Conducting polymer nanowire-based chemiresistive biosensor for the detection of bacterial spores, Biosens. Bioelectron. 25 (2010) 2309–2312.
[23] J. Gong, L. Wang, L. Zhang, Electrochemical biosensing of methyl parathion pesticide based on acetylcholinesterase immobilized onto Au–polypyrrole interlaced network-like nanocomposite, Biosens. Bioelectron. 24 (2009) 2285–2288.
[24] S. Rajesh, A.K. Koteswararao, B. Kalpana, G. Ilavazhagan, S. Kotamraju, C. Karunakaran, Simultaneous electrochemical determination of superoxide anion radical and nitrite using Cu, ZnSOD immobilized on carbon nanotube in polypyrrole matrix, Biosens. Bioelectron. 26 (2010) 689–695.
[25] S. Rajesh, U.S.E. Arivudainambi, S. Raja Singh, A. Rajendran, S. Kotamraju, C. Karunakaran, Superoxide anion radical biosensor using self-assembled cysteine monolayer on gold nanoparticles in polypyrrole matrix facilitated electron transfer in Cu, ZnSOD, Sensor Lett. 8 (2010) 1–9.
[26] D. Ueda, R. Kato, T. Kurita, H. Kamata, S. Inokuchi, S. Umemura, S. Hirono, O. Niwa, Efficient direct electron transfer with enzyme on a nanostructured carbon film

fabricated with a maskless top-down UV/ozone process, J. Am. Chem. Soc. 133 (2011) 4840–4846.
[27] W. Feng, J. Peijun, Enzymes immobilized on carbon nanotubes, Biotechnol. Adv. 29 (2011) 889–895.
[28] M.E. Ghica, R. Pauliukaite, O.F. Filho, C.M.A. Brett, Application of functionalised carbon nanotubes immobilised into chitosan films in amperometric enzyme biosensors, Sens. Actuators B 142 (2009) 308–315.
[29] P. Raveendran, J. Fu, S.L. Wallen, A simple and "green" method for the synthesis of Au, Ag, and Au–Ag alloy nanoparticles, Green Chem. 8 (2005) 34–38.
[30] Z. Zhang, L. Huang, V.M. Shulmeister, Y.I. Chi, K.K. Kim, L.W. Hung, A.R. Crofts, E.A. Berry, S.H. Kim, Electron transfer by domain movement in cytochrome bc_1, Nature 392 (1998) 677–684.
[31] T.A. Link, The role of the "Reiske" iron sulfur protein in the hydroquinone oxidation (Q_P) site of the cytochrome bc_1 complex, FEBS Lett. 412 (1997) 257–264.
[32] J.H. Nett, C. Hunte, B.L. Trumpower, Changes to the length of the flexible linker region of the Rieske protein impair the interaction of ubiquinol with the cytochrome bc_1 complex, Eur. J. Biochem. 267 (2000) 5777–5782.
[33] A.R. Crofts, The cytochrome bc_1 complex: Function in the context of structure, Annu. Rev. Physiol. 66 (2004) 689–733.
[34] F.J.M. Verhagen, T.A. Link, W.R. Hagen, Electrochemical study of the redox properties of [2Fe-2S] ferredoxins: Evidence for superreduction of the Rieske [2Fe-2S] cluster, FEBS Lett. 361 (1995) 75–78.
[35] J. Hirst, Elucidating the mechanisms of coupled electron transfer and catalytic reactions by protein film voltammetry, Biochem. Biophys. Acta 1757 (2006) 225–239.
[36] A. Mulkidjanian, Ubiquinol oxidation in the cytochrome bc_1 complex: Reaction mechanism and prevention of short-circuiting, Biochem. Biophys. Acta 1709 (2005) 5–34.
[37] M.C. Puig, X.M. Berbel, R. Rouillon, C.C. Blanchard, J. Marty, Development of a cytochrome *c* based screen-printed biosensor for the determination of the antioxidant capacity of orange juices, Bioelectrochemistry 76 (2009) 76–80.
[38] L. Guo, D. Pietkiewicz, E.V. Pavlov, S.M. Grigoriev, J.J. Kasianowicz, M.L. Dejean, J.S. Korsmeyer, B. Antonsson, W.K. Kinnally, Effects of cytochrome *c* on the mitochondrial apoptosis-induced channel MAC, Am. J. Physiol. Cell Physiol. 286 (2004) 1109–1117.
[39] C. Karunakaran, D. Aggarwal, R.Q. Migrino, J. Joseph, D. McAllister, E.V. Konorev, W.E. Antholine, J. Zielonka, S. Srinivasan, N.G. Avadhani, B. Kalyanaraman, Doxorubicin inactivates myocardial cytochrome *c* oxidase in rats: Cardioprotection by mito-Q, Biophys. J. 96 (2009) 1388–1398.
[40] R. Lüpertz, W. Watjen, R. Kahl, Y. Chovolou, Dose- and time-dependent effects of doxorubicin on cytotoxicity, cell cycle and apoptotic cell death in human colon cancer cells, Toxicology 271 (2010) 115–121.
[41] B. Kalyanaraman, J. Joseph, S. Kalivendi, S. Wang, E.A. Konorov, Doxorubicin-induced apoptosis: Implications in cardiotoxicity, Mol. Cell. Biochem. 234 (235) (2002) 119–124.